SUPPORTING INFORMATION

Influence of the Ge content on the lithiation process of crystalline $Si_{1-x}Ge_x$ nanoparticles-based anodes for Li-ion battery

Diana Zapata Dominguez[a], Christopher L. Berhaut[b], Praveen Kumar[a,e], Pierre-Henri Jouneau[b], Antoine Desrues[d], Nathalie Herlin-Boime[d], Nathalie Boudet[f], Nils Blanc[f], Gilbert A. Chahine[g], Cédric Haon[c], Samuel Tardif[a], Sandrine Lyonnard*[b], and Stéphanie Pouget*[a]*

AUTHOR ADDRESS

[a] University Grenoble Alpes, CEA, CNRS, IRIG, MEM, F-38000 Grenoble
[b] University Grenoble Alpes, CEA, CNRS, IRIG, SyMMES, F-38000 Grenoble
[c] University Grenoble Alpes, CEA, Liten, F-38000 Grenoble
[d] University Paris-Saclay, CNRS, CEA, NIMBE, 91191 Gif-sur-Yvette
[e] Shared Instrumentation Facility, Colorado School of Mines, Golden, CO, United States
[f] University Grenoble Alpes, CNRS, Inst. NEEL, F-38054 Grenoble, France
[g] University Grenoble Alpes, CNRS, Grenoble INP, SIMAP, F-38054 Grenoble, France

S1: Characterization of the crystalline pristine powders

Figure S1a and b show the complete probed scattering angle diffractogram of the Ge-rich and Si≈Ge alloy, which exhibit broad peaks, corresponding to heterogeneities in the structural composition. For the Ge-rich and Si≈Ge alloy, four and two different $Si_{1-x}Ge_x$ compositions have to be considered to account for the diffraction profile, respectively, with average Ge content $\langle x \rangle = 0.79 \pm 0.05$ and $\langle x \rangle = 0.53 \pm 0.05$.

c-Si Nps were characterized in pristine powder using X-ray powder diffraction. Figure S1c shows in red the obtained diffracted pattern. Rietveld refinement on the diffracted pattern is performed, assuming a diamond structure with a single phase with space group *Fd-3m*. The obtained lattice parameter was a = 5.428(1) Å^{-1}. The average size for the particles is 26 ± 2 nm. However, BET measurements performed on this powder have revealed a mean particle size of 71 nm.[1] The powder is probably formed by particles with an amorphous shell and a crystalline core of 26 nm. The important amorphous contribution is corroborated in the Raman spectrum on this sample.[1]

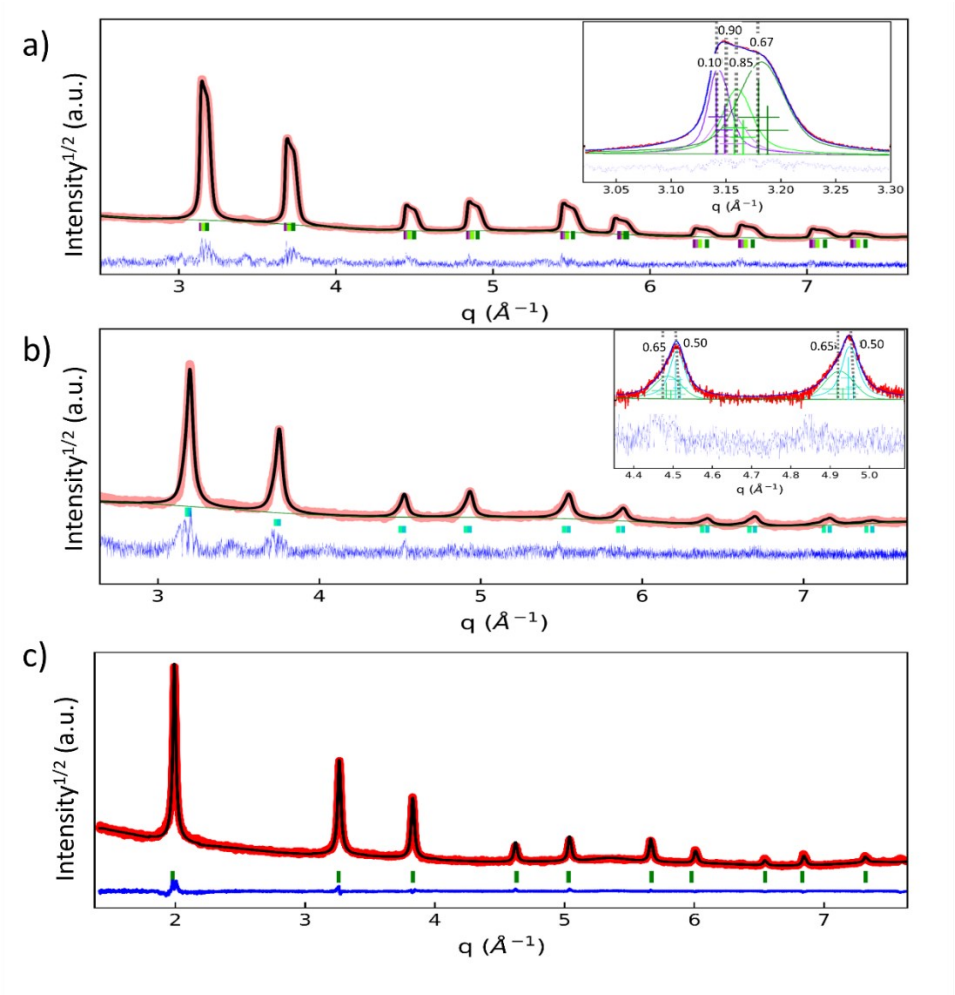

Figure S1. Rietveld refinement of the X-ray powder diffraction data of the crystalline powders a) Ge-rich alloy ($Si_{0.23}Ge_{0.77}$), b) Si≈Ge alloy ($Si_{0.53}Ge_{0.47}$), and c) Si Nps. Refined patterns (black) overlapped the observed patterns (red). The difference between the calculated and the experimental is shown in blue. The intensity is presented in the squared root scale.

S2: Complementary HRTEM and EDX mapping images of $Si_{1-x}Ge_x$ alloys

Figure S2a – d shows additional HRTEM and EDX mapping images on the Ge-rich ($Si_{0.23}Ge_{0.77}$) alloy, mostly spherical and faceted, with sizes ranging between 105 – 180 nm. Figure S2d shows the EDX chemical mapping of Figure S2c, where the Si-richer outer zone is no longer observed (see Figure S2b). Here Si and Ge are observed uniformly through the particle. We notice in Figure S2b and d that some of the particles have a core-shell structure while others have a more uniform distribution of Si and Ge. One possible reason for these differences is the synthesis method and condition. The nanoparticle synthesis is achieved by using different fractions of SiH_4 and GeH_4 as precursors for obtaining the x SiGe compositions, radiated by CO_2 laser in He/H_2; the latter is a product of the SiH_4 dissociation. The temperature of the reactive medium is higher than the stability domain of the obtained alloy composition (i.e., 1483 K > 1390 K, for $Si_{0.53}Ge_{0.47}$). In addition, a He/H_2 atmosphere in the reactive medium enables silicon migration to the particle surface. Therefore, conditions for segregation and composition migration are favored, allowing the formation of other compositional distributions and core-shell structures.[2]

Figure S2e – f shows additional HRTEM and EDX mapping images on the Si≈Ge ($Si_{0.53}Ge_{0.47}$) alloy of the nanoparticles, mostly spherical and faceted with a bimodal distribution of nanoparticle sizes as small as 50 nm and larger sizes between 70 – 150 nm. Figure S2e shows the inner and outer zones with a sharp interface with differences in intensity. The intensity strongly depends on the atomic number of the elements and the thickness of the sample. We also observed partially crystalline particles, such as the one in Figure S2g, of about 75 nm diameter. Figure S2h shows that the crystallographic planes in the interior of the particles are closer to Ge with approximate values of 3.29 Å.

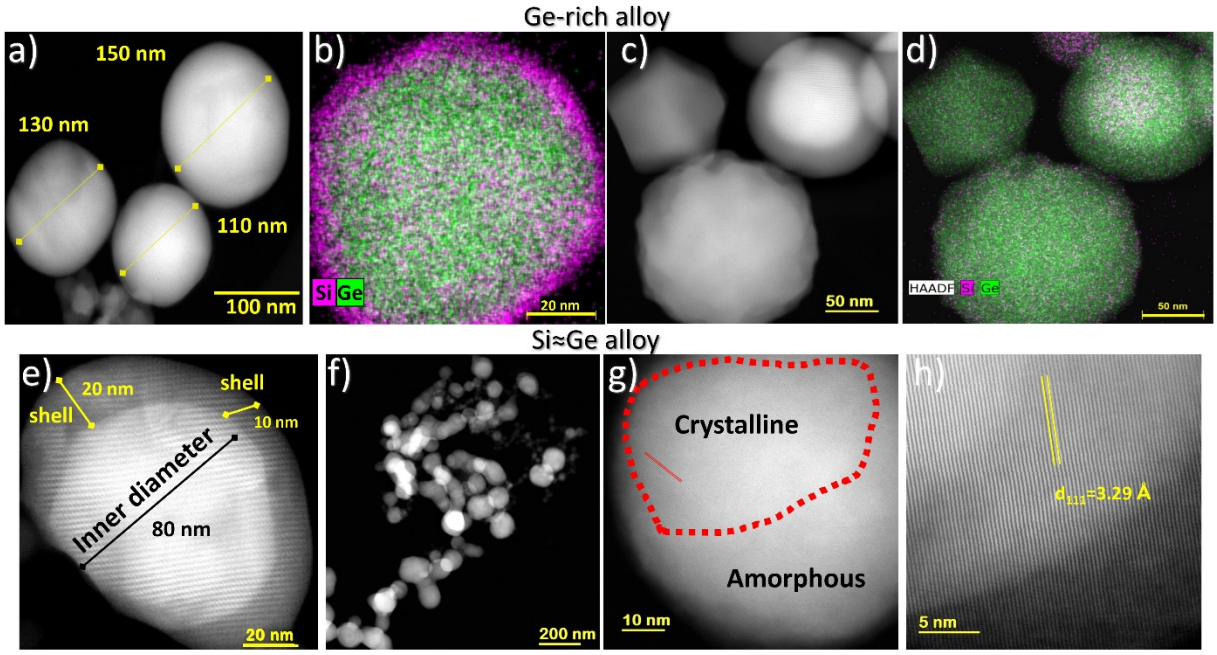

Figure S2. Additional HAADF-STEM images and STEM-EDX mapping show the morphology and element distribution for Ge-rich alloy (a –d) and for the almost equivalent in composition Si≈Ge alloy (e–h).

S3: Quantitative analysis of the SiGe(111) reflection during lithiation

Figure S3 a, b, and c show the Lorentzian functions used for the single peak refinement for Ge-rich ($Si_{0.23}Ge_{0.77}$), Si≈Ge ($Si_{0.53}Ge_{0.47}$), and Si-rich alloys, respectively, as described in the characterization of the pristine materials.

Performing a full pattern LeBail type analysis would have been complicated in the synchrotron data considering the weak relative SiGe signal. For the lab data, it would have been necessary to consider different heights for the different Be and SiGe contributions, as this has been done for pure Ge.[3] However, given the complicated structure of the SiGe compounds and the weak electrode signal, compared to pristine powder, we use single peak fitting. In the case of Si≈Ge ($Si_{0.53}Ge_{47}$) and Si-rich alloys, we had to consider a bumpy background from the pouch-cell components. Specifically, the bump at 1.875 Å comes from the separator.

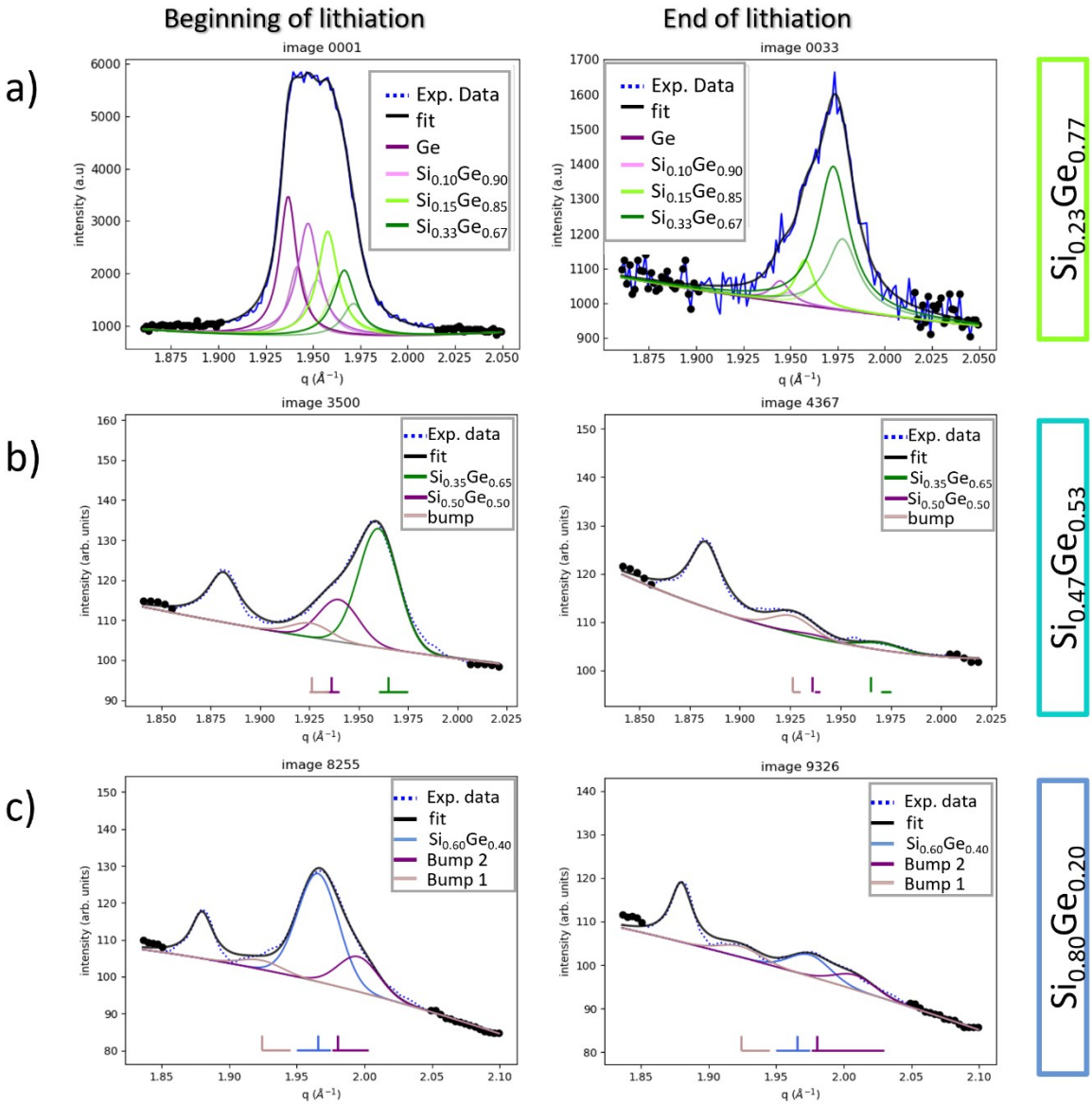

Figure S3. Single profile fitting results for the (111) reflection in a) Ge-rich alloy ($Si_{0.23}Ge_{0.77}$), considering four phases, b) Si≈Ge alloy ($Si_{0.53}Ge_{0.47}$) considering two phases, and c) Si-rich considering one crystalline phase ($Si_{0.60}Ge_{0.40}$), at the beginning and ending of lithiation.

Figure S4 shows an example of the *operando* electrochemistry data and the single peak refinement results for the four $Si_{1-x}Ge_x$ component phases of the Ge-rich alloy ($Si_{0.23}Ge_{0.77}$). The decrease of the integrated intensity is associated with the disappearance of the crystalline phase due to the lithiation. Figure 4b confirms that the lithiation voltage increases with the Ge content, varying

from 0.26 V for Ge to about 0.18 V. These results evidence the sequential lithiation of the different $Si_{1-x}Ge_x$ component phases presented in the Ge-rich alloy.

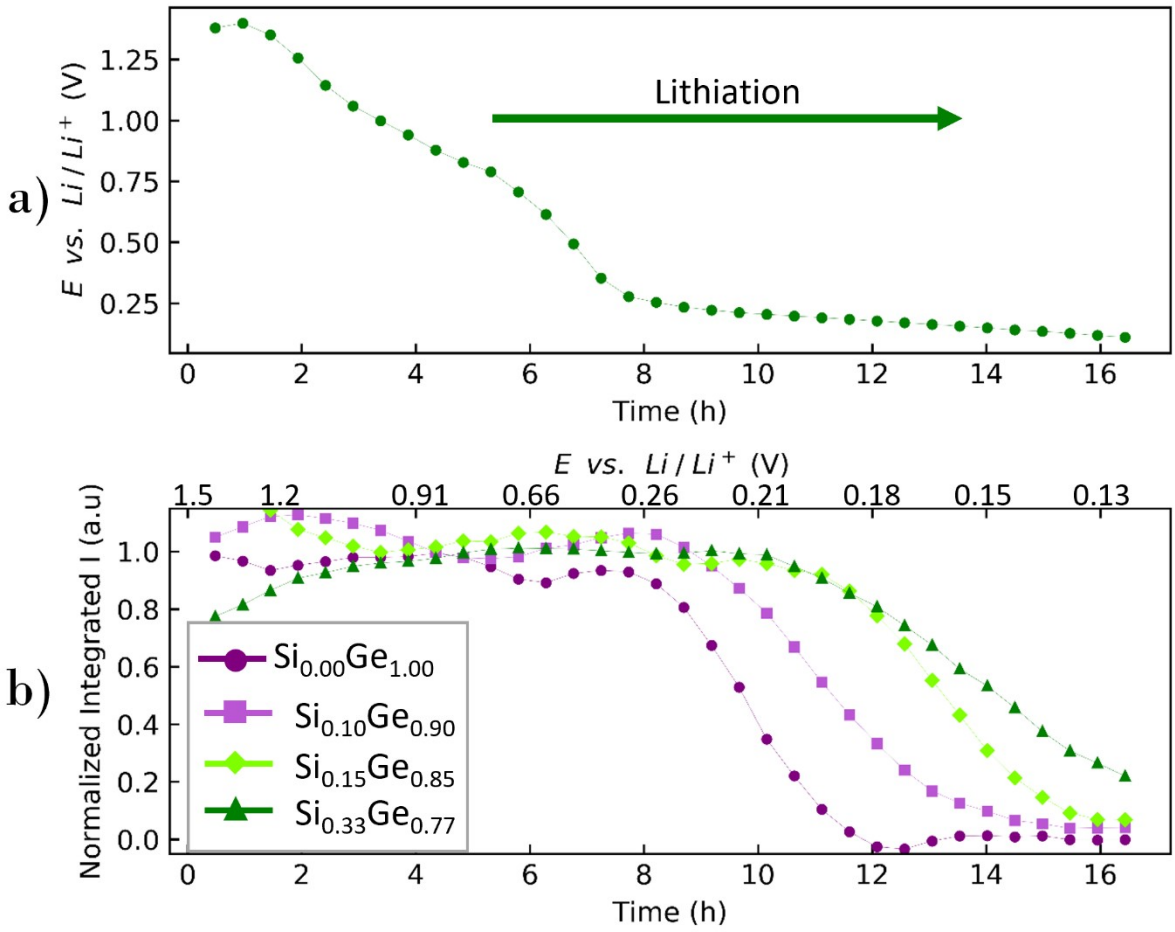

Figure S4. a) Voltage Li/Li^+ against time for the complete lithiation of the Ge-rich alloy ($Si_{0.23}Ge_{0.77}$). b) Normalized integrated intensity obtained from the fit of the four distinct phases in Ge-rich alloy *vs*. time during a complete lithiation.

Figure S5a shows the first lithiation for the crystalline Si≈Ge alloy Nps with an average composition: $Si_{0.53}Ge_{0.47}$ *vs.* Li metal down to 0.005 mV at C/20. Note that this Figure was plotted until 0.108 V. Beyond the intensity is too weak to be refined, Figure S5b shows the normalized integrated intensity against voltage that results from the fit of $Si_{0.53}Ge_{0.47}$(111) reflection during lithiation. An example of the different phases must be considered to account for the peak. In this case, phases (x = 65 and x = 50) allow describing the broad peak of the alloy with an average

composition $Si_{0.53}Ge_{0.47}$. As expected, the Ge-rich $Si_{0.23}Ge_{0.77}$ alloy decreases faster than the $Si_{0.50}Ge_{0.50}$ in the voltage range between 0.300 and 0.130 V.

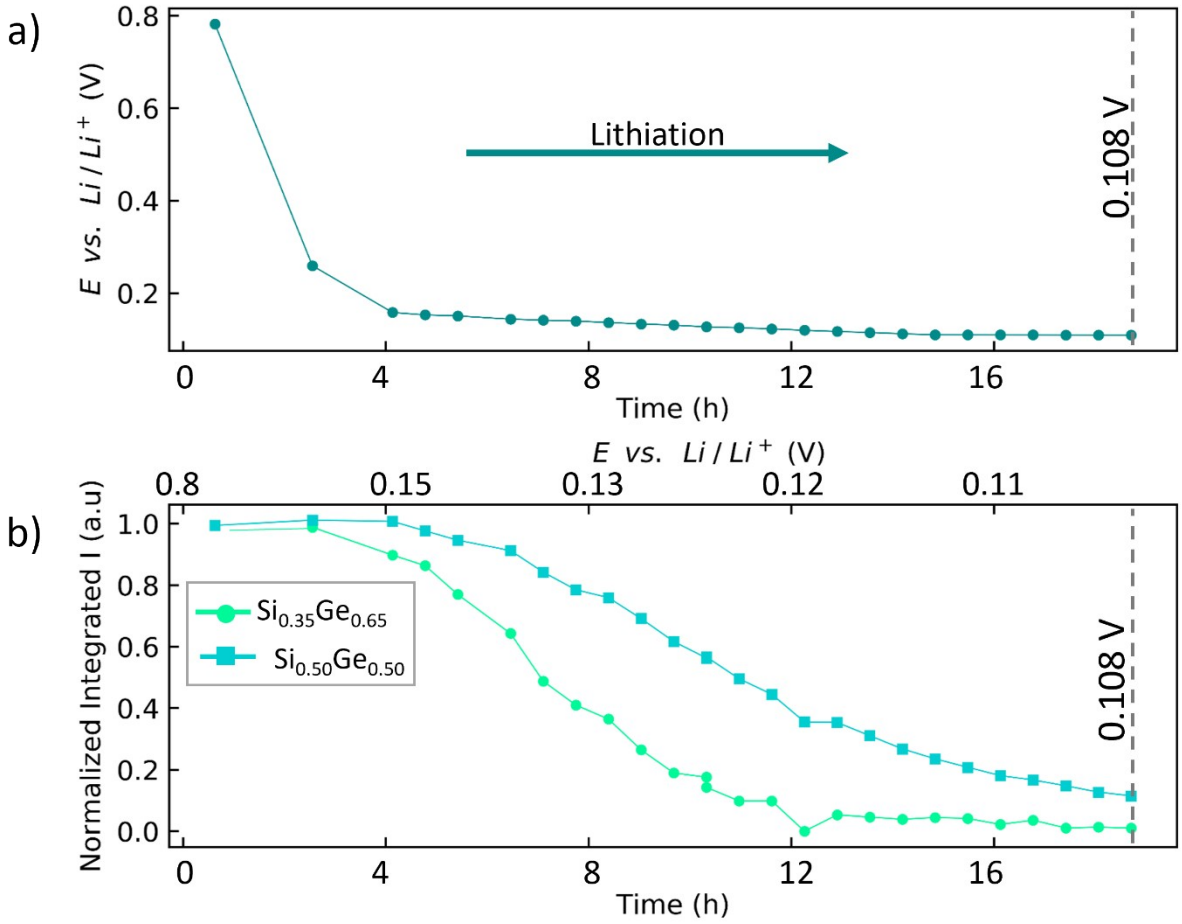

Figure S5. a) Voltage *vs.* Li/Li^+ against time for the complete lithiation of the Si≈Ge alloy with average composition $Si_{0.53}Ge_{0.47}$. b) Normalized integrated intensity obtained from the fit of the distinct phases in $Si_{0.53}Ge_{0.47}$ during a complete lithiation time.

Figure S6a and b show the time dependence of the electrochemical lithiation and the normalized integrated intensity that results from the fit of the crystalline peak $Si_{0.60}Ge_{0.40}(111)$, respectively. This compound appears to be less heterogeneous than the two others as one phase allows describing the broad peak of the alloy with an average crystalline composition $Si_{0.60}Ge_{0.40}$. This composition determined by XRD concerns only the crystalline component. As Raman scattering

on this Si-rich alloy suggests an amorphous organization,[1] we must consider that the Ge content estimated from XRD is overestimated.

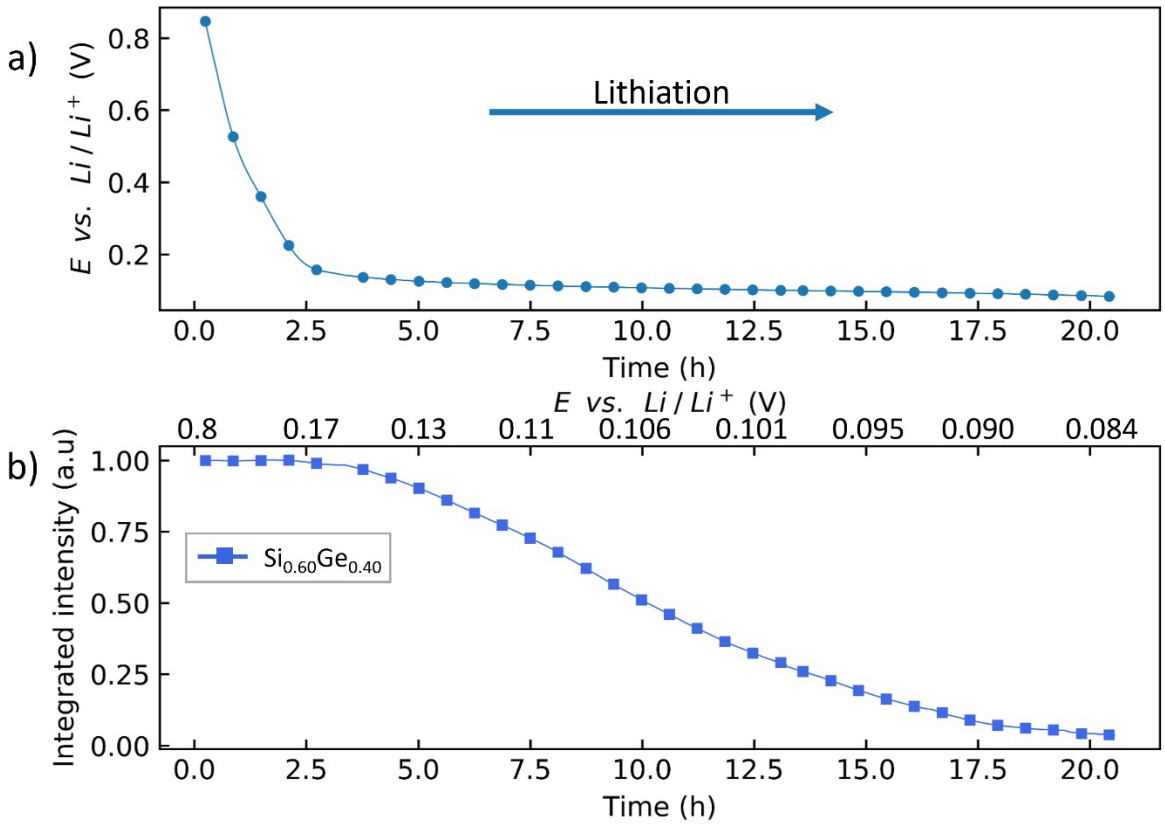

Figure S6. a) Voltage *vs.* Li/Li+ against time for the complete lithiation of the alloy with average composition $Si_{0.60}Ge_{0.40}$. b) Normalized integrated intensity obtained from the fit of $Si_{0.60}Ge_{0.40}$ during a complete lithiation time.

We also performed similar *operando* measurements with a crystalline Si Nps self-supported electrode. Figure S7a and b show respectively the electrochemical lithiation and the normalized integrated intensity against time that results from the fit of Si(111) reflection during lithiation. Crystalline Si Nps are amorphized during lithiation between 0.041 and 0.034 V *vs.* Li/Li^+.

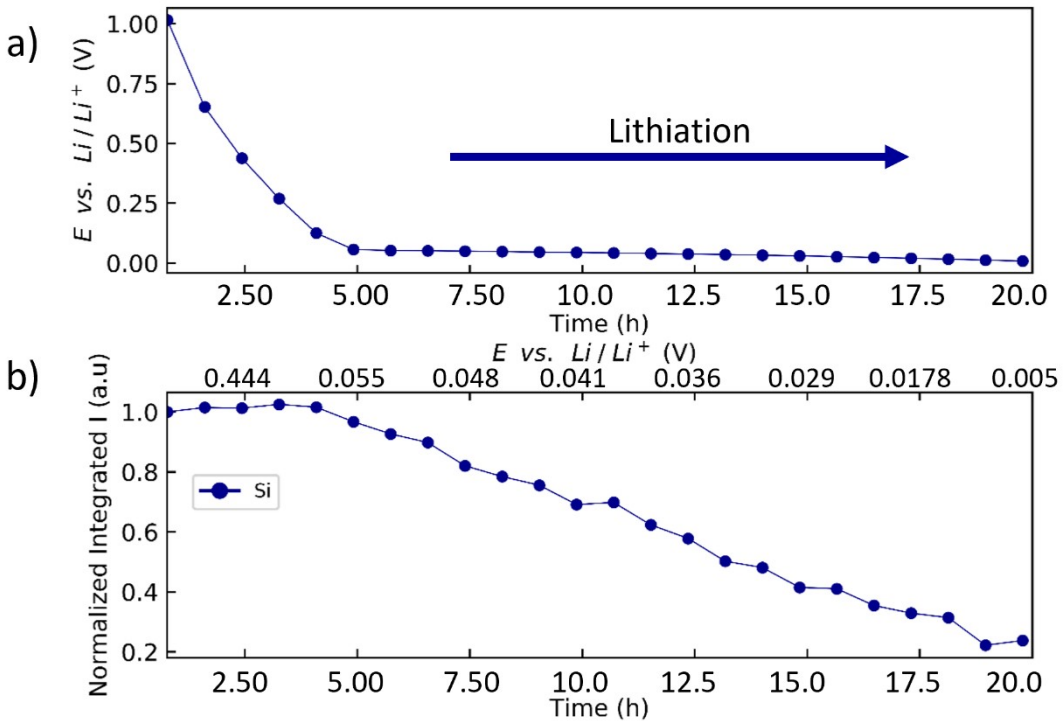

Figure S7. a) voltage *vs*. Li/Li$^+$ against time for the complete lithiation of crystalline Si Nps. b) Normalized integrated intensity obtained from the fit of Si Nps during a complete lithiation.

S4: Formation of the phases $Li_{15}(Si_{1-x}Ge_x)_4$

We follow whether the Si-rich alloy forms crystalline $Li_{15}(Si_{1-x}Ge_x)_4$. Figure S8 corroborates the absence of diffraction peaks associated with $Li_{15}(Si_{1-x}Ge_x)_4$ in the XRD patterns recorded during lithiation and delithiation of the Si-rich alloy measured in-lab as a self-supported electrode at C/20. This result is coherent with the dQ/dV curve obtained from galvanostatic cycling, which is very similar to the case of Si Nps for which c-$Li_{15}Si_4$ does not form.

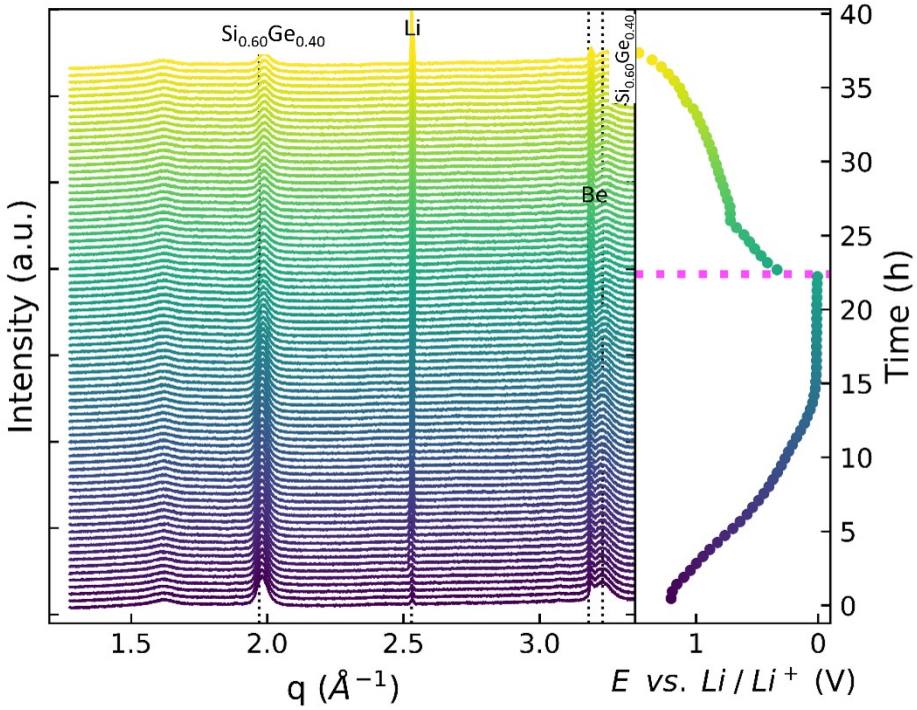

Figure S8. left: *Operando* XRD patterns, right: electrochemical cycling during the complete lithiation of Si-rich alloy at C/20.

S5: Quantitative analysis of the $Li_{15}(Si_{1-x}Ge_x)_4$ during cycling

Figure S9 shows examples of the single peak refinement on the $Li_{15}Ge_4$ (220) and $Li_{15}(Si_{1-x}Ge_x)_4$ (220) Bragg reflection for the a) pure germanium and the SiGe alloys: b) the Ge-rich and c) equivalent in composition Si≈Ge alloy The fitting was performed considering Lorentzian functions because performing a full pattern LeBail type analysis would have been complicated in the synchrotron data considering the weak relative $Li_{15}(Si_{1-x}Ge_x)_4$ signal.

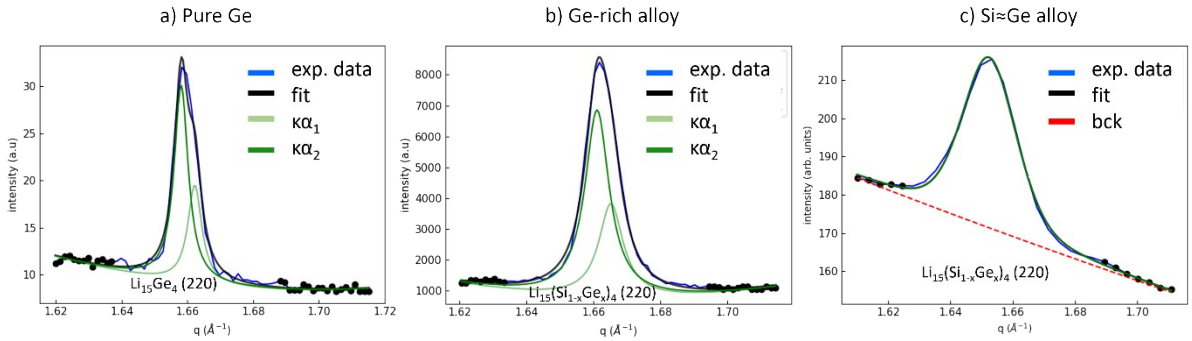

Figure S9. Single profile fitting results for the $Li_{15}Ge_4$(220) formed in a) pure germanium, and the $Li_{15}(Si_{1-x}Ge_x)_4$ formed in b) Ge-rich and c) Si≈Ge alloys.

The evolution of peak intensity, full widths at half maximum (FWHM), and the lattice parameter calculated from the $Li_{15}Ge_4$ and $Li_{15}(Si_{1-x}Ge_x)_4$ Bragg reflections (211), (220), and (310) was plotted along time to understand the evolution of these phases along cycling. These results are presented hereafter for the pure Ge (Figure S10), Ge-rich alloy (Figure S11), and Si≈Ge alloy (Figure S12.)

Figure S10a–d shows the voltage *vs*. Li/Li^+, normalized integrated intensity, full widths at half maximum (FWHM), and lattice parameter against time in hours, respectively, for the crystalline $Li_{15}Ge_4$ formed in the pure Ge cycling. For clarity, the time (hours) was replaced by the corresponding voltage. The gray dotted vertical line represents the end of lithiation.

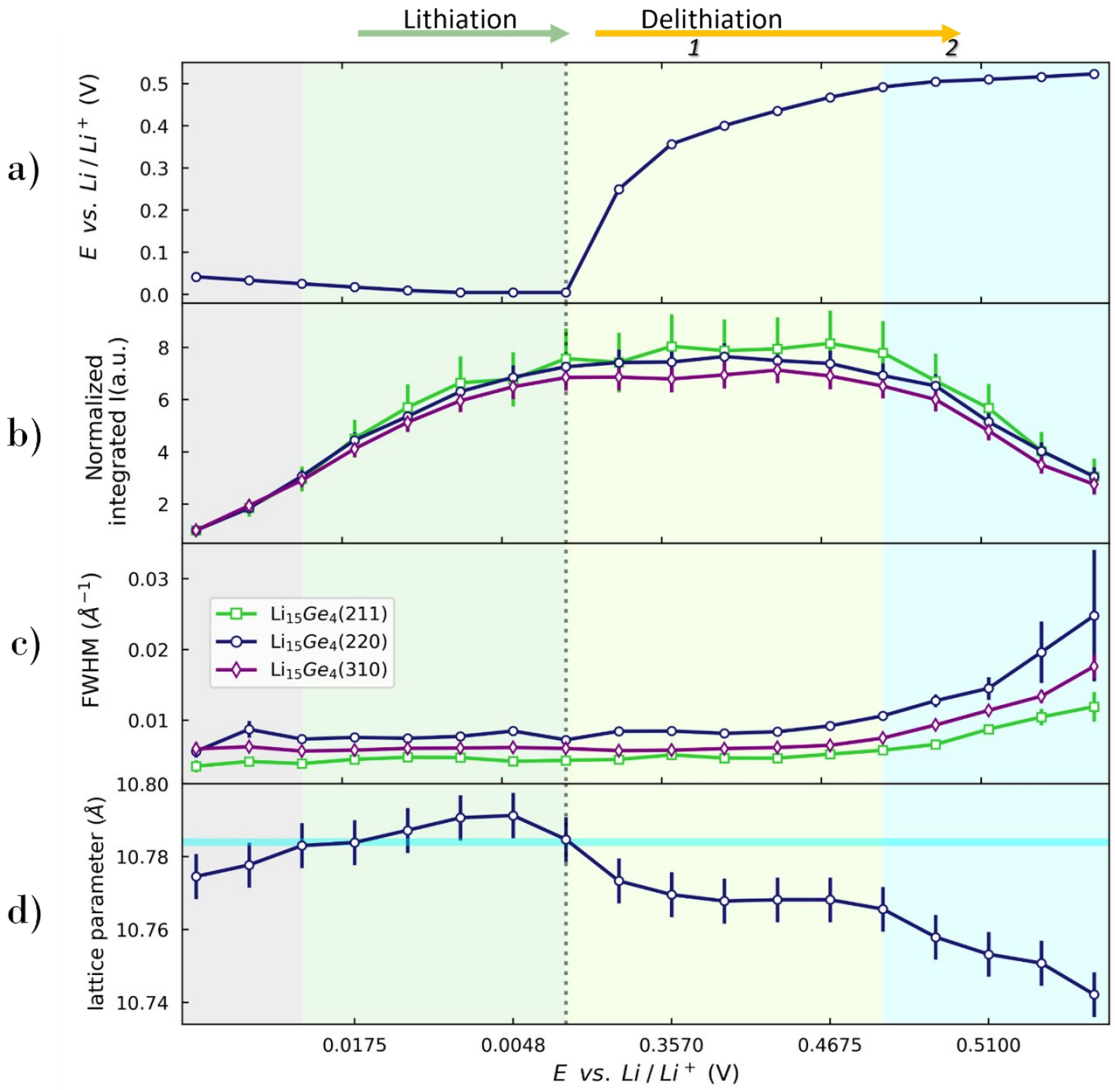

Figure S10. a) voltage *vs*. Li/Li$^+$ b) Intensity c) FWHM for the mentioned reflections, and d) Lattice parameter for the obtained $Li_{15}Ge_4$ from the pure Ge self-supported electrode during lithiation/delithiation. Note that here, time was replaced by the corresponding voltage *vs*. Li/Li$^+$.

During lithiation beyond 0.04 V, the crystalline $Li_{15}Ge_4$ phase is formed. The amount of $Li_{15}Ge_4$, which is proportional to the diffraction peak integrated intensity, increases until the end of lithiation at 0.005 V *vs*. Li/Li$^+$. The full widths at half maximum (FWHM) for the $Li_{15}Ge_4$ reflections are constant, and the lattice parameter shows a slight increase during lithiation.

Through delithiation, there are two different processes: 1) the beginning of delithiation until 0.49 V, and 2) from 0.49 V until 0.53 V. In the first stage, while the voltage is increasing considerably, the normalized integrated intensity and the FWHM stay constant. However, the lattice parameter first decreases rapidly (until ~ 10.79 $Å^{-1}$) and then stays constant. In the second process, the voltage is almost constant. In this plateau, the $Li_{15}Ge_4$ peak intensities decrease, and the FWHM increase, indicating a progressive disappearance of $Li_{15}Ge_4$.

Figure S11a–d shows the voltage *vs.* Li/Li^+, normalized integrated intensity, full widths at half maximum (FWHM), lattice parameter against time in hours, respectively, for the crystalline $Li_{15}(Si_{1-x}Ge_x)_4$ formed in the Ge-rich alloy-based anode cycling. For clarity, the time (hours) was replaced by the corresponding voltage. The gray dotted vertical line represents the end of lithiation.

During lithiation beyond 0.03 V, the crystalline $Li_{15}(Si_{1-x}Ge_x)_4$ phase is formed. The amount of $Li_{15}(Si_{1-x}Ge_x)_4$, which is proportional to the diffraction peak integrated intensity, increases until the end of lithiation at 0.005 V *vs.* Li/Li^+. The full widths at half maximum (FWHM) for the $Li_{15}(Si_{1-x}Ge_x)_4$ reflections are constant, and the lattice parameter shows a slight increase during lithiation.

Through delithiation, there are two different processes: 1) the beginning of delithiation until 0.44 V, and 2) from 0.44 V until 0.51 V. In the first stage, while the voltage is increasing considerably, the normalized integrated intensity and the FWHM stay constant. However, the lattice parameter first decreases rapidly (until ~ 10.75 $Å^{-1}$) and then stays constant. In the second process, the voltage is almost constant. In this plateau, the $Li_{15}(Si_{1-x}Ge_x)_4$ peak intensities decrease, and the FWHM increase, indicating a progressive disappearance of $Li_{15}(Si_{1-x}Ge_x)_4$. This lattice parameter behavior

during the delithiation is similar to the $Li_{15}Ge_4$ phase published by our group.[3] The $Li_{15}(Si_{1-x}Ge_x)_4$ phase obtained with the $Si_{0.53}Ge_{0.47}$ compound also has similar behavior, as shown hereafter.

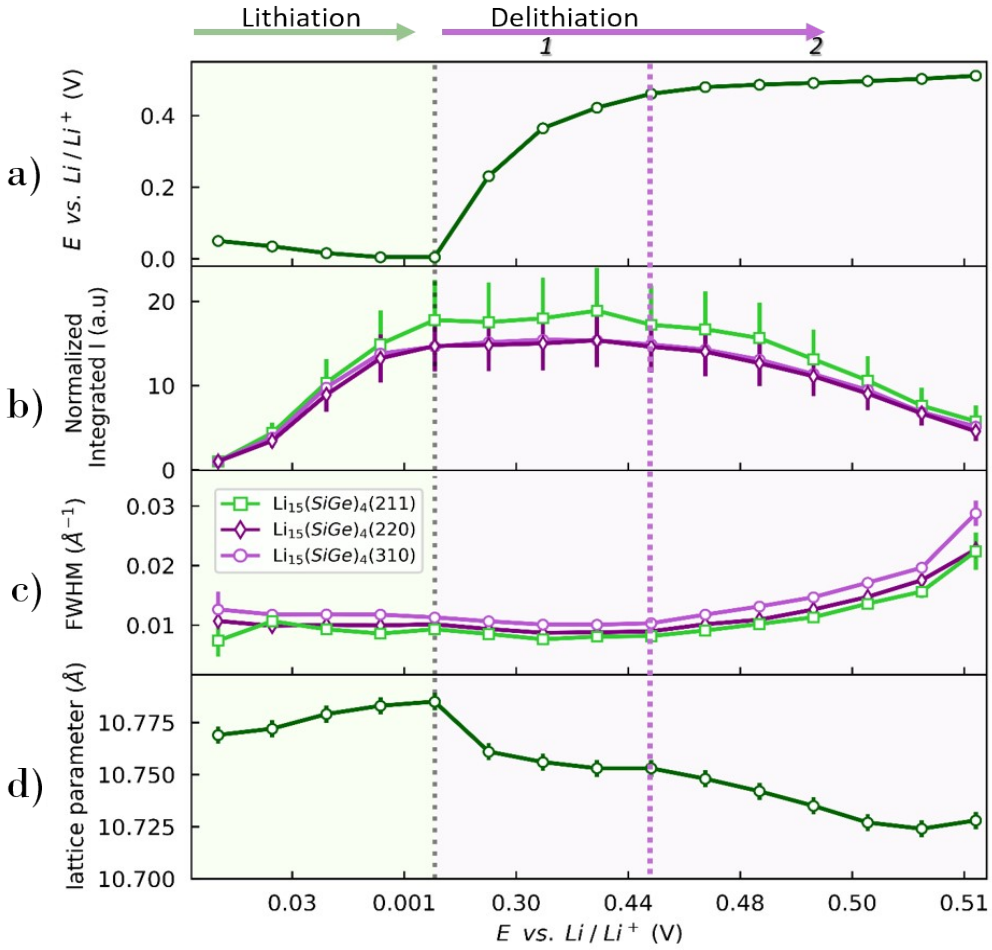

Figure S11 a) voltage *vs*. Li/Li$^+$ b) Intensity c) FWHM for the mentioned reflections, and d) Lattice parameter for the obtained $Li_{15}(Si_{1-x}Ge_x)_4$ from the Ge-rich ($Si_{0.23}Ge_{0.77}$) self-supported electrode during lithiation/delithiation. Note that here, time was replaced by the corresponding voltage *vs.* Li/Li$^+$.

Figure S12a–d shows the voltage *vs.* Li/Li$^+$, normalized integrated intensity, full widths at half maximum (FWHM), and lattice parameter for the crystalline $Li_{15}(Si_{1-x}Ge_x)_4$ formed in the Si≈Ge alloy-based anode cycling. For clarity, the time (hours) was replaced by the corresponding voltage, and the dotted vertical line represents the end of the lithiation.

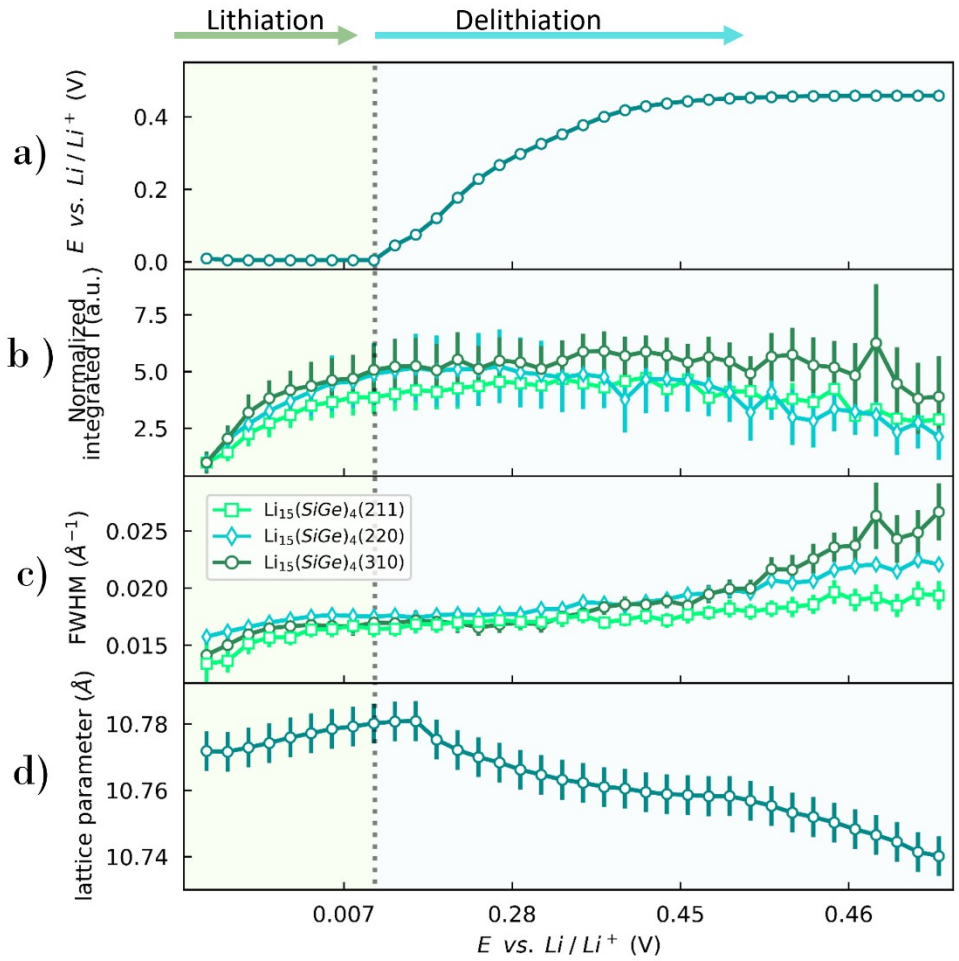

Figure S12 a) electrochemical cycling of the self-supported electrode with the almost equivalent in composition alloy *vs.* Li metal during lithiation/delithiation. b) Intensity of the $Li_{15}(Si_{1-x}Ge_x)_4$ Bragg reflections (211), (220), and (310). c) FWHM for the mentioned reflections, and d) lattice parameter *vs.* time. Note that here, time was replaced by the corresponding voltage *vs.* Li/Li$^+$.

During lithiation beyond 10 mV, the crystalline $Li_{15}(Si_{1-x}Ge_x)_4$ phase is formed. The associated diffraction intensity continues to grow until the end of lithiation at 0.005 V *vs.* Li/Li$^+$, while the full widths at half maximum (FWHM) for the different Bragg peaks are constant, and the lattice parameter shows a slight increase. During delithiation, two different stages can be distinguished: the first part of delithiation until 0.455 V and the second, from 0.455 V to 0.465 V. Through the first process, while the voltage increases considerably, the normalized integrated intensity and FWHM of the $Li_{15}(Si_{1-x}Ge_x)_4$ reflections stay constant. In contrast, the lattice parameter gradually

decreases. During the second stage, the voltage is almost constant. In this plateau, the diffraction intensity decreases. The increase in FWHMs, which is more marked for the peaks at larger scattering angles, is characteristic of an increasing distortion in the lattice. The lattice parameter evolution is similar to the one observed for the $Li_{15}Ge_4$ phase for Ge as published by our group[3] and the $Li_{15}(Si_{1-x}Ge_x)_4$ for $Si_{0.23}Ge_{0.77}$.

Figure 13 shows the evolution of the (220) FWHM of the c-$Li_{15}(Si_{1-x}Ge_x)_4$ phase as a function of the voltage formed in pure Ge, Ge-rich, and Si≈Ge compounds.

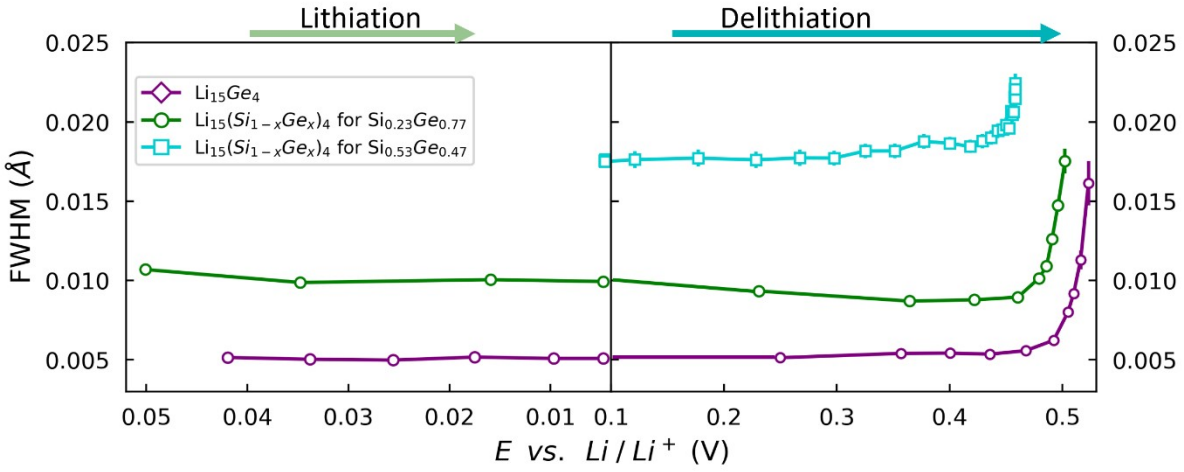

Figure S13. FWHM as a function of voltage *vs.* Li/Li^+ during lithiation and delithiation for the $Li_{15}(Si_{1-x}Ge_x)_4$ phase obtained with Ge, $Si_{0.23}Ge_{0.77}$, and $Si_{0.53}Ge_{0.47}$ compounds.

References

(1) Desrues, A.; Alper, J. P.; Boismain, F.; Zapata Dominguez, D.; Berhaut, C.; Coulon, P.-E.; Soloy, A.; Grisch, F.; Tardif, S.; Pouget, S.; Lyonnard, S.; Haon, C.; Herlin-Boime, N. Best Performing SiGe/Si Core-Shell Nanoparticles Synthesized in One Step for High Capacity Anodes. *Batter. Supercaps* **2019**, *2* (12), 970–978. https://doi.org/10.1002/batt.201900094.

(2) Kim, H.; Son, Y.; Park, C.; Lee, M.-J.; Hong, M.; Kim, J.; Lee, M.; Cho, J.; Choi, H. C. Germanium Silicon Alloy Anode Material Capable of Tunable Overpotential by

Nanoscale Si Segregation. *Nano Lett.* **2015**, *15* (6), 4135–4142. https://doi.org/10.1021/acs.nanolett.5b01257.

(3) Zapata Dominguez, D.; Berhaut, C. L.; Buzlukov, A.; Bardet, M.; Kumar, P.; Jouneau, P.-H.; Desrues, A.; Soloy, A.; Haon, C.; Herlin-Boime, N.; Tardif, S.; Lyonnard, S.; Pouget, S. (De)Lithiation and Strain Mechanism in Crystalline Ge Nanoparticles. *ACS Nano* **2022**, *16* (6), 9819–9829. https://doi.org/10.1021/acsnano.2c03839.